Advances in Water Resources 31 (2008) 1382–1386

Contents lists available at ScienceDirect

Advances in Water Resources

journal homepage: www.elsevier.com/locate/advwatres

Residence time of bedform-driven hyporheic exchange

M. Bayani Cardenas [a,*], John L. Wilson [b], Roy Haggerty [c]

[a] Department of Geological Sciences, The University of Texas at Austin, Austin, TX 78712, United States
[b] Earth and Environmental Sciences, New Mexico Institute of Mining and Technology, Socorro, NM 87801, United States
[c] Department of Geosciences, Oregon State University, Corvallis, OR 97331, United States

ARTICLE INFO

Article history:
Received 19 March 2008
Received in revised form 4 June 2008
Accepted 10 July 2008
Available online 19 July 2008

Keywords:
Power-law residence time distribution
Hyporheic zone
Bedform
Sediment–water interface
Interfacial exchange zone

ABSTRACT

Biogeochemical and ecological transformations in hyporheic zones are dependent on the timing of hyporheic exchange. We show through linked modeling of open channel turbulent flow, groundwater flow, and solute transport that the residence time distributions of solutes advected by hyporheic flow induced by current–bedform interaction follow power-laws. This tailing behavior of solutes exiting the sediments is explained by the presence of multiple path lengths coupled with very large variability in Darcy flow velocity, both occurring without heterogeneity in sediment permeability. Hyporheic exchange through bedforms will result in short-time fractal scaling of stream water chemistry.

1. Introduction

The cause of observed residence time distributions (RTDs) of transient storage in streams remains unclear. The persistence of this enigma over decades [1,18,21,23,25] generates uncertainty regarding the role of streams as integrators of watershed processes and hampers interpretation of tracer tests which are typical tools for understanding stream and hyporheic processes. Transient storage of water occurs in the hyporheic zone and in zones of zero net downstream advection within channels or dead zones. In-channel transient storage RTDs have been found to be exponential [10,24,25]. Exponential RTDs for hyporheic exchange are also assumed when applying a one-dimensional transient storage model, based on first-order exchange, for estimation of exchange parameters [19]. However, recent evidence shows that not all transient storage has an exponential RTD. Persistence of stream tracer skewness in both space and time cannot be explained by a simple exponential model [21]. A log-normal RTD was found in the hyporheic zone of a low-gradient stream [26]. Haggerty et al. [12] and Gooseff et al. [9,10] found power-law RTDs that may be associated with hyporheic exchange, although recent data (Haggerty data, unpublished) suggest that rate-limited tracer desorption may be responsible for the results. Haggerty et al. [12] suggested that a power-law distribution of transient storage may be responsible for early-time fractal scaling in time-series of bulk-stream solute concentrations recorded by Kirchner et al. [16].

The RTDs of pore water in sediment determine which ecological functions and biogeochemical transformations will or will not take place in sediment [2,13,22]. For many processes, timing is everything. However, hyporheic RTDs are controlled by the presence of multiple pathways controlled by current–topography interaction (e.g. [8]), stream geomorphology (e.g. [5,15]) and heterogeneity in the hydraulic conductivity of sediments (e.g. [3]). Therefore, it is very challenging to extract a detailed mechanistic basis for fitted RTDs from in-stream tracer tests since it provides a collective signal. Elliott and Brooks [7] showed that RTDs of solutes pumped through ripples have a form that, although not noted in the publication, results in a power-law tail. They assumed a flat boundary at the top of the bed (i.e., the sediment–water interface) and flow in the vertically semi-infinite domain was driven by sinusoidal pressure distribution along the flat top boundary [7]. More recently, Wörman et al. [27] analyzed three-dimensional hyporheic exchange through a streambed by imposing a Fourier representation of streambed topography, translating it to a dynamic pressure distribution and imposing it as a boundary condition on a flat surface. Their particle tracking analysis resulted in a bimodal RTD which they attribute to two distinct wavelengths of bedforms. However, it is crucial that the actual shape and surface of the bedforms are included in models as fast flowpaths through the bedforms are excluded from the "flat surface" formulations [4]. Marion et al. [17] show that exchange models excluding the shapes of bedforms may not be able to accurately represent exchange through

* Corresponding author. Tel.: +1 512 471 6897.
E-mail address: cardenas@mail.utexas.edu (M. Bayani Cardenas).

0309-1708/$ - see front matter © 2008 Elsevier Ltd. All rights reserved.
doi:10.1016/j.advwatres.2008.07.006

bedforms protruding significantly into the water column. We recently showed that for the case of a single bedform shape (and hydraulic parameters) that the RTD for bedform-driven hyporheic exchange follows a power-law [5].

Cardenas and Wilson [4] have shown that the hyporheic flow fields through bedforms are sensitive to bedform morphology. We further explore what we found recently by investigating RTDs for different triangular bedform morphology. RTDs for current–bedform driven transport through hyporheic zones are generated directly via modeling of turbulent flow over triangular bedforms and linking this to groundwater and solute transport models of the underlying sediment.

2. Methods

We follow the approach in [4]. Mean unidirectional turbulent flow in the water column over subaqueous two-dimensional dunes is simulated by solving the Reynolds-averaged Navier–Stokes (RANS) equations with the k–ω closure scheme. The RANS-derived pressure along the sediment–water interface (SWI), which is considered a no-slip wall for the water column, is prescribed as a Dirichlet boundary for the groundwater flow domain resulting in sequential coupling of flow in the water column and in the underlying sediments. The top of the water column is a symmetry boundary. The bottom of the sediments is prescribed as a no-flow boundary. Lateral boundaries are considered spatially periodic with the same prescribed pressure drop for both the water column and the sediments. The pressure drop, dP, results in mean flow from left to right of the domain. The modeling scheme is illustrated in Fig. 1. Detailed discussion of the hydrodynamics and validation of the modeling formulation is available in Cardenas and Wilson [4].

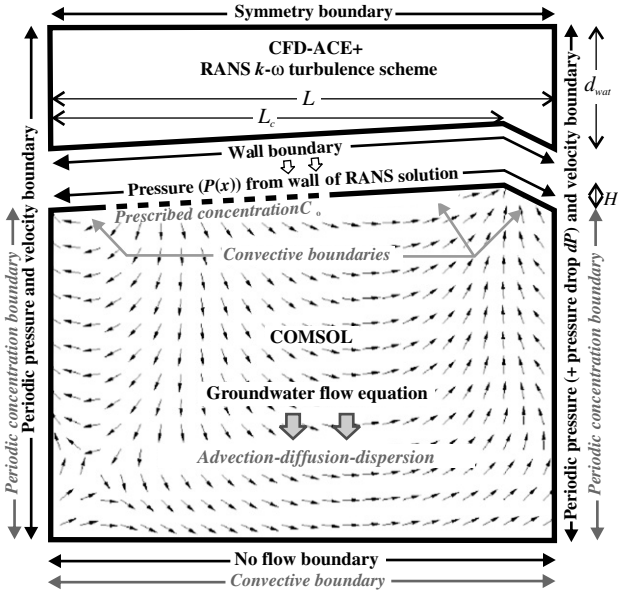

Fig. 1. Numerical modeling formulation (modified after [4]). Top part shows the model boundary conditions for the turbulent flow model. Bottom part illustrates boundary conditions for groundwater flow (black lines and text) and solute transport models (gray lines and italicized text). Arrows in bottom figure indicate flow directions. Domains are vertically truncated with only the lowermost portion of the water column and the uppermost portion of the sediments shown; the entire domain is 1.2 m deep. The governing equations are solved sequentially in the following order: (1) RANS–k–ω, (2) groundwater flow equation, and (3) solute advection–diffusion–dispersion. L = 1.0 m, H = 0.05 m, d_{wat} = 0.5 m, and V_{ave} = 0.17 m/s in all simulations. L_c/L = 0.9 in the figure but actual values vary from 0.5 to 0.9 in the simulations.

The advection–diffusion–dispersion equation for solute transport:

$$\frac{\partial C}{\partial t} = D_m \frac{\partial^2 C}{\partial x_i^2} + \frac{\partial}{\partial x_i}\left(D_{ij}\frac{\partial C}{\partial x_i}\right) - u_i \frac{\partial C}{\partial x_i} \quad (1)$$

where C is solute concentration, t is time, D_m is the molecular diffusion coefficient in porous media, and u is the pore velocity. Index i, j = 1, 2. D, the mechanical dispersion coefficient tensor is defined as follows [6]:

$$D_{ij} = \alpha_T U \delta_{ij} + (\alpha_L - \alpha_T) u_i u_j / U \quad (2)$$

where α_T and α_L are transverse and longitudinal dispersivities, U is the pore velocity magnitude, and δ_{ij} is the Kronecker delta function. α_L is varied from 0.1 to 10 cm covering a broad range of values including those typical for the scale of our experiments (e.g. [6]). α_T is considered to be 1/10 of α_L. D_m is set at 5×10^{-11} m^2/s which is typical for geologic materials [14]. The dispersion coefficient is 5–250 times that of the diffusion coefficient in our experiments.

The SWI is divided into in-flow and out-flow zones based on the distribution of Darcy velocity normal to the SWI. The dividing point between these two zones corresponds to a "hinge-line" in the velocity distribution. The in-flow zone assumes a Dirichlet condition (prescribed concentration) following step injection:

$$C = 0 \ (\text{mol/m}^3) \quad \text{for } t < 0 \text{ s} \quad (3)$$

$$C = C_0 = 100 \ (\text{mol/m}^3) \quad \text{for } t \geqslant 0 \text{ s} \quad (4)$$

while the out-flow zones along the sediment–water interface are convective boundaries (i.e. Neumann condition with zero dispersive flux):

$$\frac{\partial C}{\partial n} = 0 \quad (5)$$

where n is the direction normal to the boundary.

The RANS equations are numerically solved using the finite-volume approach as implemented in the code CFD-ACE+. The groundwater flow and solute transport equations are solved using the finite-element method implemented in COMSOL Multiphysics. Lagrange–Quadratic triangular elements are used in COMSOL Multiphysics with node spacing less than 2 cm. The governing equations are sequentially solved in the following order: (1) RANS–k–ω, (2) groundwater flow equation, (3) solute transport equation.

We ran simulations with each simulation corresponding to a different bedform asymmetry, L_c/L, where L_c is the horizontal location of the crest relative to the entire length of the bedform (Fig. 1) and three dispersivity values. L_c/L = 0.5 is a symmetric dune while L_c/L = 0.9 is more typical of an angle-of-repose dune. In all simulations, the bedform length L = 1.0 m, the bedform height H = 0.05 m, the depth of the sediments below the trough is 1.2 m (previous studies shows that at this depth, the location of this boundary is inconsequential [4]), the water column depth along the trough d_{wat} = 0.5 m and the average horizontal velocity, V_{ave}, taken above the crest is 17 cm/s. The sediments are assigned a permeability of 2×10^{-10} m^2 which is roughly equivalent to well-sorted coarse sand to gravel. Dense spacing is maintained throughout the unstructured finite-element mesh with triangular elements to limit numerical dispersion. The node spacing along the top boundary is 0.5 cm and the node spacing within the domain is 1 cm. This resulted in more than 50,000 elements in the domain that is 1 m wide and 1.2 m deep. Numerical dispersion is minimized at this resolution and there is no grid-dependence of the solution. Solute transport simulations typically took several CPU hours but usually less than a day on a single-processor workstation.

3. Results and discussion

Thorough validation and discussion of the flow modeling scheme can be found in [4] and is not repeated here. Please refer to that manuscript for details.

The breakthrough-curves (BTCs) are derived by integrating the flux-weighted concentrations at the out-flow zones across the SWI designated as convective boundaries (Fig. 1). The integral of flux-weighted C is normalized by the integrated flux-weighted concentration (C_0) across the in-flow zones designated as a prescribed concentration boundary in Fig. 1. Flux-weighed concentration is the resident concentration at a point along a boundary multiplied by the fluid flux across it. For a step-input, the BTC is equivalent to the residence time cumulative distribution function (CDF).

Different bedform asymmetry will result in different CDFs even though the forcing is similar (Fig. 2), i.e., the Reynolds number (and average velocity) for the current that induces the circulation through the sediments is the same. Different bedform asymmetry results in different pressure distributions along the SWI (see Fig. 8c in [4]) which results in similarly variable groundwater flow fields (see Fig. 7b in [4]). Of particular interest is the relative size of the two flow cells in the sediments (one circulating counter-clockwise or towards the downstream direction and the other circulating clockwise or towards the upstream direction). When L_c/L is around 0.7–0.9, the streamlines near the SWI from the inflow point to the main out-flow at the crest for the two flow cells are of different lengths. The clockwise-circulating cell has shorter flow-lengths. Based on visual inspection, the case with $L_c/L = 0.8$ has the shortest flow-length, resulting in the earliest substantial breakthrough observed in Fig. 2. The flow-lengths for $L_c/L = 0.7$ and 0.9 are similar but appear to be slightly longer than that for $L_c/L = 0.8$ resulting in slightly delayed breakthrough. The flow-lengths for more symmetric bedforms with $L_c/L = 0.5$ and 0.6 are longer, with $L_c/L = 0.5$ the longest, thereby resulting in later breakthrough. The left column in Fig. 2 corresponds to cases with minimal dispersion. The BTCs for this case are therefore more reflective of transport primarily driven by the variable groundwater flow field. Increasing the longitudinal dispersivity (the dispersivity increases 10-fold each column towards the right in Fig. 2) makes the BTC shapes more similar, reflecting the diminished effect of the variable flow field and increased dispersive effects.

Haggerty et al. [12] and Gooseff et al. [9] suggested that the late-time portion of BTCs yields significant information regarding hyporheic exchange and that characterization of long-timescale hyporheic exchange is critical to biogeochemical studies. Our simulations show that late-time breakthrough may differ solely due to bedform asymmetry. The case $L_c/L = 0.8$, with the steepest BTC at early time, flattens at a higher relative concentration which suggests that pathlines corresponding to long or even infinite residence times are less dominant. On the other hand, the case with $L_c/L = 0.9$ results in flattening of the BTC at a smaller relative concentration suggesting increased importance of long residence times.

The derivatives of the residence time CDFs give the probability density functions or RTDs and are presented in Fig. 2. The RTDs again illustrate the differences in early-time behavior but most importantly show that at later times, all cases converge to a power-law RTD across two-orders of magnitude change in dispersivity. Regression of power-law models to the RTDs based on visually constrained time periods results in practically perfect fits (Table 1). The time-duration of this power-law behavior slightly varies for different L_c/L, with more asymmetric bedforms entering this power-law behavior at later times compared to those with smaller L_c/L (Table 1). The power-law behavior is observed across more than two-orders of magnitude change in time and may persist to more than 100 days. (Our simulations are for sand–gravel systems but the duration of the power-law behavior can be scaled linearly with the permeability of the sediments owing to and within the limits of Darcy's Law.) A characteristic residence time or turnover time, τ, can be computed from the area and flux (Table 1). Flux and area are computed following Cardenas and Wilson [4]. Values for τ decrease with increasing asymmetry. The power-law RTD persists up to many times that of τ since most of the flushing occurs at shallower depths.

Our simulations provide a direct and mechanistic explanation for observed power-law RTD (e.g. [9,12]) which have also been considered as an explanation for fractal behavior in stream solute concentrations (e.g. [16]). The power-law behavior is driven by the wide distribution of flowpaths and residence-times within the interfacial exchange zone. There are infinitesimally short advective flowpaths along the "hingeline" and there are relatively very long flowpaths, the longest of which intersect stagnation zones. In fact, these two flowpaths are translated to an infinitesimally short and infinitely long residence times; that is, if we ignore the impact of dispersion (numerical and actual). Moreover, velocity decreases quasi-exponentially with distance from the SWI. All these factors lead to a strongly heterogeneous groundwater flow field that is responsible for the RTD. The stagnation zones, which are found where the gray streamlines in Fig. 7 from [4] intersect, are partly responsible for the heavy tails in the BTCs. The effects of stagnation zones are analogous to the no-slip wall conditions for viscous flow through a pipe with no entropy-driven transport which results in a RTD that is proportional to t^{-3}, indicating a finite-mass/infinite-residence-time behavior. We expect our RTDs to have a power greater than -2 since transport is not purely advective, i.e., we consider dispersion and diffusion. In fact, Table 1 shows that the exponents in the fitted models are between -1.82 and -1.96. We compared the diffusive/dispersive flux to the advective flux in the out-flow areas in order to assess the relative significance of advection and diffusion/dispersion, on the resulting RTD. At the early-time limits used in our regression (see Table 1), the advective fluxes through the SWI are 2–3 orders of magnitude larger than that for combined diffusion/dispersion. Diffusive/dispersive fluxes get even smaller relative to advective fluxes through time. The power-law RTD at late-times is dominantly generated by the current–bedform induced hyporheic flow field rather than diffusive/dispersive processes.

Increasing the dispersivity clearly affects the early-time behavior and may delay the onset of a late-time power-law RTD. But in some cases, large dispersion may also result in a distinguishable early-time power-law with a smaller exponent (see cases with $\alpha_L = 0.1$ m in Fig. 2). This transition from one power-law RTD to another occurs at smaller dispersion coefficients for more asymmetric bedforms ($\alpha_L = 0.01$ m, $L_c/L = 0.8$, 0.9). The suite of simulation results in Fig. 2 illustrates the relative importance of macrodispersion and a non-dispersive but strongly variable groundwater flow field on generating power-law RTDs. However, their absolute individual contribution is impossible to distinguish. For these cases, we surmise that extreme dispersion may result in early-time power-law breakthrough while a strongly variable groundwater flow field is more important in generating late-time power-law tailing. The exponents for the early-time and late-time power-laws are different and this may be a promising characteristic for distinguishing which process is more important.

Several models have been used to describe the RTDs of hyporheic zones based on in-stream tracer experiments that record integrated signals. The resulting RTDs are determined by which process dominates, and these processes may vary in space and time. Exponential distributions are expected where exchange with

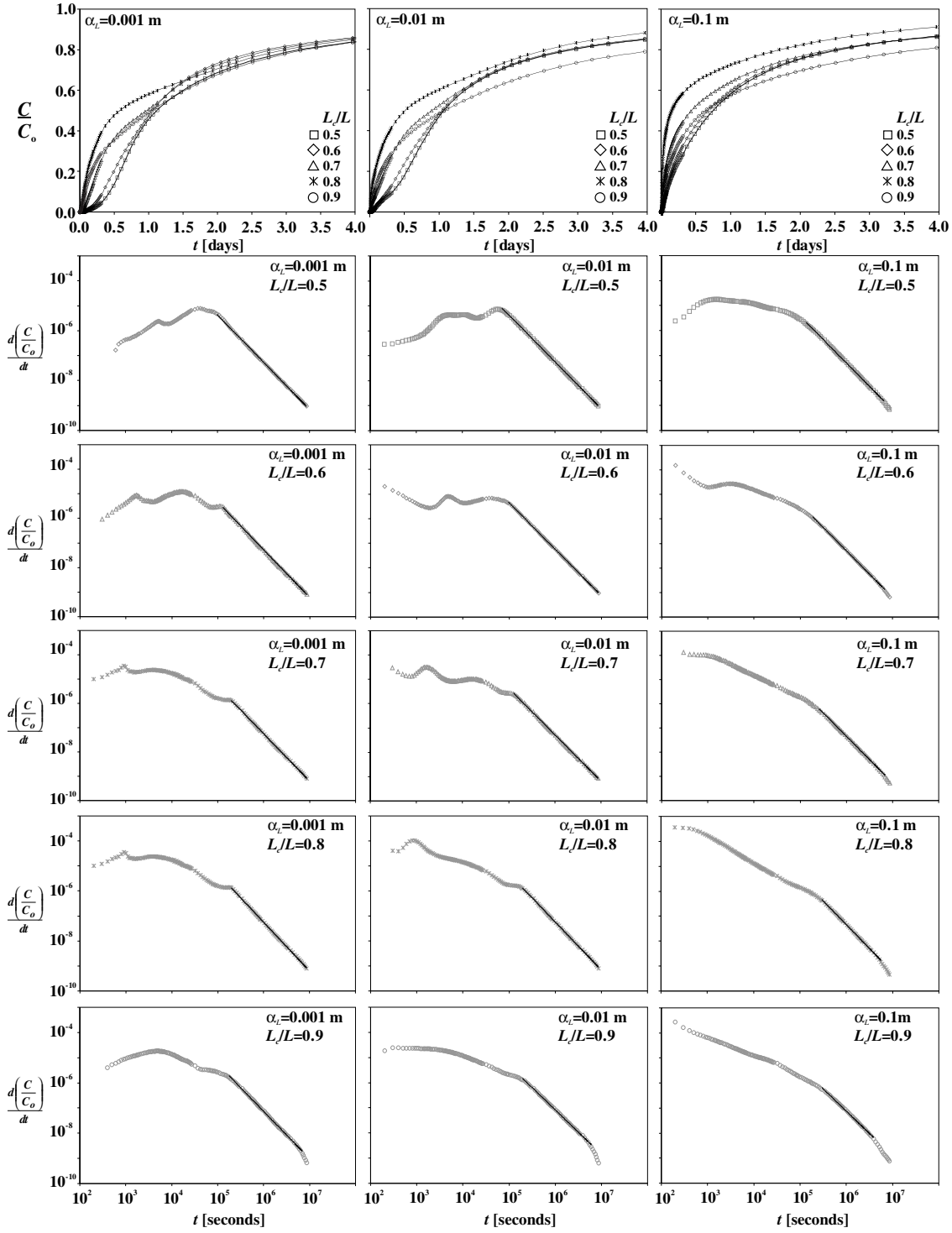

Fig. 2. Top row: early-time residence-time distribution cumulative distribution function (CDF), which for a step injection is equivalent to the breakthrough curves (BTCs). The RTDs for the different simulations are presented in the lower rows. Power-law models are fitted to the RTDs; regression results are presented in Table 1. Sediment permeability $k_p = 2 \times 10^{-10}$ m^2, average water column velocity $V_{ave} = 0.17$ m/s, bedform height $H = 0.05$ m, and bedform length $L = 1$ m for all simulations. Longitudinal dispersivity, α_L, increases 10-fold from left to right. Bedform asymmetry increases by 0.1 from top to bottom.

transient storage zones can be characterized by diffusive-type processes. However, transient storage modeling where exponential models are prescribed is sensitive only to early-time portions of RTDs [11]. Perhaps, in such previous studies, the exchange processes over which the tracers are monitored are dominated by factors other than current–bedform induced exchange, which we show results in power-law RTDs, or perhaps other factors are indeed dominant even at later times. Exchange through heterogeneous streambeds has been shown to result in different types of RTDs. For example, Cardenas et al. [3] showed that RTDs of solutes through heterogeneous streambeds are log-normal while Saenger et al. [20] presented examples of bimodal distributions. Moreover, Cardenas et al. [3] illustrated that log-normal RTDs may be generated solely by spatially variable hydraulic conductivity without the

Table 1
Hyporheic exchange measures and power-law ($d(C/C_0)/dt = at^b$) regression parameters

L_c/L	Flux (m^2/d)	Area (m^2)	τ (days)	α_L = 0.001 m		α_L = 0.01 m		α_L = 0.1 m	
				b	R^2	b	R^2	b	R^2
0.5	0.070	0.873	12.50	−1.944	0.9984	−1.896	0.9998	−1.857	0.9992
0.6	0.072	0.873	12.12	−1.948	0.9994	−1.916	0.9999	−1.870	0.9994
0.7	0.074	0.856	11.53	−1.990	0.9998	−1.954	0.9998	−1.882	0.9993
0.8	0.078	0.787	10.12	−1.989	0.9992	−1.972	0.9996	−1.861	0.9991
0.9	0.064	0.685	10.74	−1.873	0.9992	−1.745	0.9991	−1.736	0.999

presence of irregular pressure distributions due to topography. (Note, however, that the RTDs in Cardenas et al. [3] are not appropriately flux-weighted). We therefore expect that in the absence of strong heterogeneity in the stream sediments and significant in-channel storage zones, but in the presence of topography along the sediment–water interface, RTDs associated with interfacial (hyporheic) exchange will follow a power-law from timescales of several minutes to tens of days. This power-law tailing is expected to be ubiquitous since bedforms tend to be self-similar across several scales [5]. Similar hyporheic flow fields may be present under non-triangular topography as long as the pressure gradients are due to variability in dynamic pressure along the sediment–water interface and not due to changes in elevation in the free water surface such as in high-Froude number flows in pool–riffle sequences. Therefore, any solute pulse introduced to a stream experiencing significant current–bedform driven interfacial exchange will be transformed to a power-law signal, lending further credibility to and a mechanistic basis for Haggerty et al.'s [12] assertion that early-time fractal behavior in stream solute chemistry (e.g. [16]) may be due to interfacial exchange.

Acknowledgements

This research was partially funded by an American Geophysical Union Horton Research Grant and a New Mexico Water Resources Research Institute Student Grant to MBC. We thank five anonymous reviewers for their helpful comments.

References

[1] Bencala KE, Walters RA. Simulation of solute transport in a mountain pool-and-riffle stream: a transient storage model. Water Resour Res 1983;19:718–24.
[2] Boulton AJ, Findlay S, Marmonier P, Stanley EH, Valett HM. The functional significance of the hyporheic zone in streams and rivers. Annu Rev Ecol Syst 1998;29:59–81.
[3] Cardenas MB, Wilson JL, Zlotnik VA. Impact of heterogeneity, bedforms, and channel curvature on hyporheic exchange. Water Resour Res 2004;40:W08307. doi:10.1029/2004WR003008.
[4] Cardenas MB, Wilson JL. Dunes, turbulent eddies, and interfacial exchange with permeable sediments. Water Resour Res 2007;43:W08412. doi:10.1029/2006WR005787.
[5] Cardenas MB. Surface-ground water interface geomorphology leads to scaling of residence times. Geophys Res Lett 2008;35:L08402. doi:10.1029/2008GL033753.
[6] de Marsily G. Quantitative hydrogeology: groundwater hydrology for engineers. Orlando: Academic Press; 1986.
[7] Elliott AH, Brooks NH. Transfer of nonsorbing solutes to a streambed with bed forms: theory. Water Resour Res 1997;33:123–236.
[8] Elliott AH, Brooks NH. Transfer of nonsorbing solutes to a streambed with bed forms: Laboratory experiments. Water Resour Res 1997;33:123–36.
[9] Gooseff MN, Wondzell SM, Haggerty R, Anderson J. Comparing transient storage modeling and residence time distribution (RTD) analysis in geomorphically varied reaches in the Lookout Creek basin, Oregon, USA. Adv Water Resour 2003;26:925–37.
[10] Gooseff MN, LaNier J, Haggerty R, Kokkeler K. Determining in-channel (dead zone) transient storage by comparing solute transport in a bedrock channel–alluvial channel sequence, Oregon. Water Resour Res 2005;41:W06014. doi:10.1029/2004WR003513.
[11] Harvey JW, Wagner BJ, Bencala KE. Evaluating the reliability of the stream tracer approach to characterize stream-subsurface water exchange. Water Resour Res 1996;32:2441–51.
[12] Haggerty R, Wondzell SM, Johnson MA. Power-law residence time distribution in the hyporheic zone of a 2nd-order mountain stream. Geophys Res Lett 2002;29:1640. doi:10.1029/2002GL014743.
[13] Huettel M, Webster IT. Porewater flow in permeable sediments. In: Boudreau BP, Jorgensen BB, editors. The benthic boundary layer: transport processes and biogeochemistry. New York: Oxford University Press; 2001.
[14] Ingebritsen SE, Sanford WE. Groundwater in geologic processes. New York: Cambridge University Press; 1998.
[15] Kasahara T, Wondzell SM. Geomorphic controls on hyporheic exchange flow in mountain streams. Water Resour Res 2003;39:1005. doi:10.1029/2002WR001386.
[16] Kirchner JW, Feng X, Neal C. Fractal stream chemistry and its implications for contaminant transport in catchments. Nature 2000;403:524–7.
[17] Marion A, Bellinello M, Guymer I, Packman AI. Effect of bed form geometry on the penetration of nonreactive solutes into a streambed. Water Resour Res 2002;38:1209. doi:10.1029/2001WR000264.
[18] Nordin CF, Troutman BM. Longitudinal dispersion in rivers: the persistence of skewness in observed data. Water Resour Res 1980;16:123–8.
[19] Runkel RL. One dimensional transport with inflow and storage (OTIS): a solute transport model for streams and rivers. US Geological Survey Water-Resources Investigation Report 98-4018. USGS, Denver; 1998.
[20] Saenger N, Kitanidis PK, Street RL. A numerical study of surface–subsurface exchange processes at a riffle–pool pair in the Lahn River, Germany. Water Resour Res 2005;41:W12424. doi:10.1029/2004WR003875.
[21] Schmid BH. Persistence of skewness in longitudinal dispersion data: can the dead zone model explain it after all? J Hydraul Eng 2002;128:848–54.
[22] Stanford JA, Ward JV. The hyporheic habitat of river ecosystems. Nature 1988;335:64–6.
[23] Thackston EL, Schnelle Jr KB. Predicting the effects of dead zones on stream mixing. J Sanit Eng Div ASCE 1970:319–31.
[24] Uijttewaal WSJ, Lehmann D, Mazijk AV. Exchange processes between a river and its groyne fields: model experiments. J Hydraul Eng 2001;127:928–36.
[25] Valentine EM, Wood IR. Longitudinal dispersion in dead zones. J Hydraul Eng 1977;103:975–90.
[26] Wörman A, Packman AI, Johansson H, Jonsson K. Effect of flow-induced exchange in hyporheic zones on longitudinal transport of solutes in streams and rivers. Water Resour Res 2002;38:1001. doi:10.1029/2001WR000769.
[27] Wörman A, Packman AI, Marklund L, Harvey JW, Stone SG. Exact three-dimensional spectral solution to surface–groundwater interactions with arbitrary surface topography. Geophys Res Lett 2006;33:L07402. doi:10.1029/2002GL025747.